A mechanism to pin skyrmions in chiral magnets

2013 J. Phys.: Condens. Matter 25 076005

(http://iopscience.iop.org/0953-8984/25/7/076005)

J. Phys.: Condens. Matter **25** (2013) 076005 (8pp) doi:10.1088/0953-8984/25/7/076005

A mechanism to pin skyrmions in chiral magnets

Ye-Hua Liu and You-Quan Li

Zhejiang Institute of Modern Physics and Department of Physics, Zhejiang University, Hangzhou 310027, People's Republic of China

E-mail: yhliu@zju.edu.cn and yqli@zju.edu.cn

Received 5 October 2012, in final form 17 December 2012
Published 22 January 2013
Online at stacks.iop.org/JPhysCM/25/076005

Abstract

We propose a mechanism to pin skyrmions in chiral magnetic thin films by introducing local maxima of magnetic exchange strength as pinning centers. The local maxima can be realized by engineering the local density of itinerant electrons. The stationary properties and the dynamical pinning and depinning processes of an isolated skyrmion around a pinning center are studied. We carry out numerical simulations of the Landau–Lifshitz–Gilbert (LLG) equation and find a way to control the position of an isolated skyrmion in a pinning center lattice using electric current pulses. The results are verified by a Thiele equation analysis. We also find that the critical current to depin a skyrmion, which is estimated to have order of magnitude 10^7–10^8 A m^{-2}, has linear dependence on the pinning strength.

(Some figures may appear in colour only in the online journal)

1. Introduction

In recent years, the topological object known as a skyrmion has been observed in chiral magnets, and attracts considerable research interest in condensed matter physics. A skyrmion is a configuration of three-dimensional unit vectors in a two-dimensional base space which wraps around the unit sphere n times, where n is the topological number. Skyrmions were first proposed in high energy physics [1] and considered as an important class of excitations in ferromagnets in condensed matter physics [2]. Recently they were theoretically predicted [3–5] and experimentally observed in the ground state configuration of chiral magnets in a magnetic field [6–9]. The skyrmions either appear as isolated objects or form a close-packed lattice. The skyrmion lattice is also observed in a single layer of magnetic metal film [10] with each skyrmion having atomic length scale. Furthermore, a multiferroic skyrmion lattice in which spin couples to an electric dipole has been reported very recently [11]. The phase diagram and the spin-wave spectrum of the skyrmion lattice in chiral magnets are well understood in the framework of a classical Heisenberg spin model with Dzyaloshinsky–Moriya (DM) interaction [3, 4, 8, 12–19].

In conducting chiral magnets, a skyrmion's topological charge becomes an emergent quantized magnetic flux from the perspective of an adiabatically moving electron. In real materials, the diameter of a skyrmion is tens of nanometers and the averaged emergent magnetic field is several teslas [20], so the coupling between the skyrmions and the conducting electrons is quite strong. It is observed that this emergent magnetic field gives rise to an anomalous Hall effect signal in the A-phase of the chiral magnet MnSi [21, 22]. The reaction of the conducting electrons to the skyrmion is the spin transfer torque [23–29]. It is predicted and observed that this torque will push the skyrmions to move in the same direction as the current [20, 23, 30]. A moving skyrmion can be considered as a moving magnetic flux, and a static magnetic field in a moving frame induces an electric field in the laboratory frame due to Faraday's law. This emergent electric field has been measured by Schulz *et al* very recently [20].

For realistic applications, it is desirable to manipulate these skyrmions in artificial devices. Very recently, Tchoe and Han showed that a circular electric current can generate skyrmions without the aid of a magnetic field [31]. Given that a skyrmion is created, another important issue is to manipulate its spacial position. Inspired by the 'magnetic domain-wall racetrack memory' [32], where artificially made pinning

centers and electric current pulses are used to manipulate the positions of magnetic domain-walls, we study the pinning and depinning effects of skyrmions.

In this paper, we propose a mechanism to pin skyrmions by introducing local maxima of the magnetic exchange strength as pinning centers. We study the effect of such a pinning center by stationary state analysis using the energy functional and dynamical analysis via both the Landau–Lifshitz–Gilbert (LLG) equation and Thiele's equation. Then we propose a method to manipulate the skyrmion's position by an electric current pulse in an artificial pinning center lattice, which may be realized by putting patterned metal grains on the surface of a chiral magnetic thin film. We organize the paper as follows. In section 2, we give the field theory description of chiral magnets and the stationary state analysis. In section 3, we formulate the dynamics of chiral magnets by the LLG equation on a square lattice and show the simulations of the dynamical pinning and depinning processes. In section 4, we give a discussion and outlook.

2. Stationary state analysis

2.1. Chiral magnet with a pinning center

The energy density for the chiral magnet is [16]

$$\mathscr{F}_{\rm tot} = \frac{J(\mathbf{r})}{2}\sum_{\mu}(\partial_\mu \mathbf{n})^2 + D(\mathbf{r})\mathbf{n}\cdot(\nabla\times\mathbf{n}) - B\,n_z, \qquad (1)$$

where $\mathbf{n}(\mathbf{r})$ represents the orientation of local magnetic moment with $\mathbf{n}^2 = 1$, $\mu = x, y, z$, $J(\mathbf{r})$ the local ferromagnetic exchange strength, $D(\mathbf{r})$ the local strength of DM interaction and B the uniform applied magnetic field. From previous works of mean-field theories and numerical simulations it is already known, for a certain range of B, that a skyrmion solution is stable [3–5, 16, 17] and the trial function for a single skyrmion is

$$\mathbf{n}(\rho,\phi,z) = \sin[\theta(\rho)]\hat{\phi} + \cos[\theta(\rho)]\hat{z}, \qquad (2)$$

where we have adopted a cylindrical coordinate system with local unit vectors $\hat{\rho}$, $\hat{\phi}$ and $\hat{z}$. θ is the angle between $\mathbf{n}$ and $\hat{z}$.

To study the pinning effect caused by inhomogeneity, we make J and D space dependent. For simplicity, we consider an axisymmetric case such that J and D are dependent merely on ρ. We choose

$$J(\rho) = J(\infty)\left\{1 + \lambda\exp\left[-\left(\frac{\rho}{\xi}\right)^2\right]\right\} \qquad (3)$$

to represent a local maximum of magnetic exchange strength. The local magnetic exchange strength is determined by the local density of itinerant electrons [30]. Here we let $D(\rho)$ and $J(\rho)$ have constant ratio $\kappa = D/(2J)$ because the density of itinerant electrons will not change the ratio of spin dependent hopping integral to spin independent hopping integral in the underlying Hubbard model. Introducing the reduced magnetic field $\beta = B/[8\kappa^2 J(\infty)]$ and scaling the space coordinate as $\rho \to (\rho/4\kappa)$, we can rewrite the energy density as

$$\frac{\mathscr{F}_{\rm tot} - \mathscr{F}_{\rm fe}}{8\kappa^2 J(\infty)} = \frac{J(\rho)}{J(\infty)}\left[\left(\frac{\partial\theta}{\partial\rho}\right)^2 + \frac{\partial\theta}{\partial\rho} + \frac{\sin^2(\theta)}{\rho^2} + \frac{\sin(\theta)\cos(\theta)}{\rho}\right] - \beta[\cos(\theta) - 1], \qquad (4)$$

where we have subtracted the energy density of the ferromagnetic state $\mathscr{F}_{\rm fe} = -B$, which corresponds to $\mathbf{n} = (0, 0, 1)$. Here we write $\theta(\rho)$ as θ for compactness. From this energy functional we construct a reduced one-dimensional functional $\mathscr{F}$, which is dimensionless and satisfies

$$\mathscr{F} = 2\pi\rho \times \frac{\mathscr{F}_{\rm tot} - \mathscr{F}_{\rm fe}}{8\kappa^2 J(\infty)}. \qquad (5)$$

To obtain the optimized function $\theta(\rho)$ that minimizes the total energy $\int_0^\infty \mathrm{d}\rho\mathscr{F}$, we construct the 'imaginary time evolution'

$$\frac{\partial\theta(\rho,\tau)}{\partial\tau} = -\left\{\frac{\partial\mathscr{F}}{\partial\theta(\rho)} - \frac{\partial}{\partial\rho}\frac{\partial\mathscr{F}}{\partial[\partial_\rho\theta(\rho)]}\right\}, \qquad (6)$$

which is a second order partial differential equation for function $\theta(\rho)$ that should be supplemented with an appropriate initial condition. The boundary condition is chosen to be [3, 4, 16]

$$\theta(0,\tau) = \pi, \qquad \theta(\infty,\tau) = 0, \qquad (7)$$

which is natural since the spins point downward at the center of a skyrmion and point upward far away from the center. To solve this equation numerically, we introduce $R_{\rm cut}$ as the numerical cut of the theoretically infinite system which should be tested to be large enough. The initial condition is chosen randomly by

$$\theta(\rho,0) = \begin{cases}\pi & \text{for } \rho = 0,\\ \text{random}(0,\pi) & \text{for } 0 < \rho < R_{\rm cut},\\ 0 & \text{for } \rho = R_{\rm cut},\end{cases} \qquad (8)$$

where random$(0, \pi)$ generates a random number ranging from zero to π. We choose $R_{\rm cut} = 50$ and slice the space interval $[0, R_{\rm cut}]$ into 1000 pieces, then we approximate the space derivative by finite difference and perform the time integral using the Runge–Kutta method. We have confirmed that $R_{\rm cut} = 50$ is large enough, that is, the results are the same for larger $R_{\rm cut}$. We numerically integrate this initial-boundary-value problem until $\theta(\rho,\tau)$ converges to a stationary function. The results for different random initial conditions are the same, so we find the global minimum of the energy functional and the globally optimized function $\theta(\rho)$.

2.2. Numerical results

Now we briefly introduce the phase diagram of a two-dimensional chiral magnet at zero temperature. For a uniform system with constant J and D in space, as we increase the magnetic field from zero, the ground state changes from the helical state to the skyrmion lattice state and then to the field polarized ferromagnetic state [3, 4, 7, 8, 16–18]. At

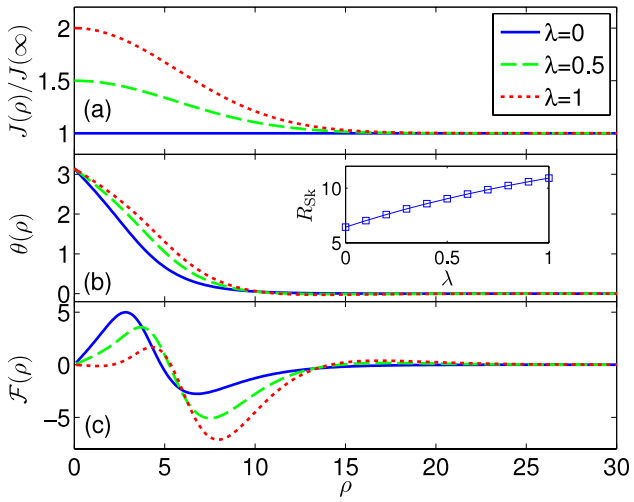

Figure 1. ρ dependence of exchange strength $J(\rho)$ (a), optimized trial function $\theta(\rho)$ (b) and energy density $\mathscr{F}(\rho)$ (c) for different pinning strengths λ. It is clearly shown that a local maximum of J lowers the core energy of a skyrmion. The inset in (b) shows the dependence of skyrmion radius on pinning strength.

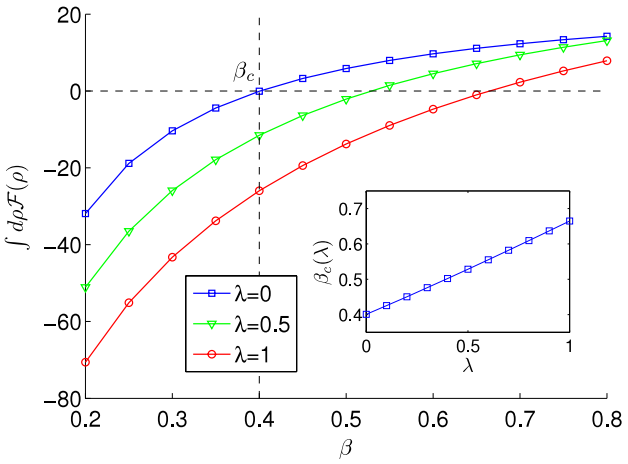

Figure 2. Single skyrmion energy versus magnetic field for different strengths of pinning center λ. It is shown that a larger strength of pinning λ gives a lower skyrmion energy $\int \mathrm{d}\rho\,\mathscr{F}$ for the same magnetic field. As a result, a larger λ makes it harder to polarize a skyrmion to the ferromagnetic state by applying magnetic field, so the critical field (in which the total energy is zero) is larger for pinned skyrmions (see inset).

the boundary between the skyrmion lattice phase and the field polarized ferromagnetic phase, an isolated skyrmion has an averaged energy density that is the same as that of the ferromagnetic state, so statistically a dilute population of isolated skyrmions is allowed. This 'skyrmion gas' state is the state of interest in the following discussion. It is worth noticing that there is a strong resemblance between this skyrmion gas and the vortices in the type-II superconductor at the lower critical magnetic field H_{c1}.

Below we show the ρ dependence of coupling J, optimized trial function $\theta(\rho)$ and energy density $\mathscr{F}$ for different parameters (figure 1). We choose $\beta = 0.4$ and $\xi = 8$ for three pinning strengths $\lambda = 0$, $\lambda = 0.5$ and $\lambda = 1$. $\beta = 0.4$ corresponds to the critical field without a pinning center. We have used $\xi = 8$ so that the size of the pinning center is comparable to the radius of the skyrmion, which is defined by $R_{Sk} = \pi[(\partial\theta/\partial\rho)_{\rho=0}]^{-1}$, thus we can make patterned pinning centers as dense as possible (see the following sections). In figure 1 it is shown that, for the uniform case $\lambda = 0$ (blue curve), the energy density profile has a positive maximum and a negative minimum in the core region of a skyrmion. At the critical field $\beta = 0.4$ the positive 'energy cost' and the negative 'energy gain' cancel each other. This is precisely the aforementioned phase boundary of the skyrmion lattice phase and the field polarized ferromagnetic phase. If there is a local maximum of coupling J for nonzero λ, the core energy is lowered (green and red curves) and the radius of the skyrmion is enlarged (inset in figure 1(b)).

Next we discuss the pinning effect in different magnetic fields (figure 2). We plot the dependence of skyrmion energy on the magnetic field for the three pinning strengths. It is shown that, for the same β, larger λ makes the energy lower, thus there can be a negative energy skyrmion in the skyrmion gas phase or even in the field polarized ferromagnetic phase. As a result, the critical magnetic field (in which the skyrmion has zero energy) is larger for a pinned skyrmion (inset in figure 2), so it is expected that pinned skyrmions can be observed in the ferromagnetic phase in real experiments.

To summarize, a pinned skyrmion becomes more stable than a 'free skyrmion' from the energy point of view. This is what we call the effect of pinning a skyrmion with a local maximum of magnetic exchange strength.

3. Dynamical analysis

3.1. Landau–Lifshitz–Gilbert equation

In section 2 we have confirmed the pinning effect from the energy point of view. To study the dynamics of the pinning process, we use the Hamiltonian which is the discrete version of equation (1) on a square lattice [16–18, 31]

$$H = \sum_{\mathbf{r},\vec{\delta}}[-J_{\mathbf{r}}\,\mathbf{S}_{\mathbf{r}}\cdot\mathbf{S}_{\mathbf{r}+\vec{\delta}} - D_{\mathbf{r}}\,\vec{\delta}\cdot(\mathbf{S}_{\mathbf{r}}\times\mathbf{S}_{\mathbf{r}+\vec{\delta}})] - B\sum_{\mathbf{r}} S^z_{\mathbf{r}}, \quad (9)$$

where $\mathbf{S}_{\mathbf{r}}$ ($\mathbf{S}_{\mathbf{r}}^2 = 1$) are local magnetic moments at positions $\mathbf{r} = (x, y)$, $x, y = -(N-1)/2, \ldots, +(N-1)/2$ for even number N, and $\vec{\delta} = \mathbf{e}_x, \mathbf{e}_y$ are two bond vectors in two dimensions. This lattice model is related to equation (1) by the standard continuum limit procedure $\sum_{\mathbf{r}} \to \frac{1}{a^2}\int \mathrm{d}x\mathrm{d}y$ with lattice constant a. The one to one correspondence of the parameters in both models follows

$$J_{\mathbf{r}} \to J(\mathbf{r}), \qquad D_{\mathbf{r}} \to aD(\mathbf{r}), \qquad B \to a^2 B. \quad (10)$$

The dynamics of this magnetic system subjected to an applied electric current is obtained by the Landau–Lifshitz–Gilbert (LLG) equation with a current term

$$\frac{\partial\mathbf{S}_{\mathbf{r}}}{\partial t} = \mathbf{S}_{\mathbf{r}}\times\mathbf{H}_{\mathrm{eff}}(\mathbf{r}) - \alpha\mathbf{S}_{\mathbf{r}}\times\frac{\partial\mathbf{S}_{\mathbf{r}}}{\partial t} - \sum_{\vec{\delta}} j_{\vec{\delta}}\mathbf{S}_{\mathbf{r}}\times\left(\frac{\mathbf{S}_{\mathbf{r}+\vec{\delta}} - \mathbf{S}_{\mathbf{r}-\vec{\delta}}}{2}\times\mathbf{S}_{\mathbf{r}}\right), \quad (11)$$

where $j_{\vec{\delta}}$ is the δ-component of the applied electric current and α the phenomenological Gilbert damping parameter. The effective magnetic field $\mathbf{H}_{\rm eff}(\mathbf{r})$ is obtained by the Hamiltonian as

$$\begin{aligned}\mathbf{H}_{\rm eff}(\mathbf{r}) &= -\frac{\partial H}{\partial \mathbf{S}_{\mathbf{r}}} \\ &= \sum_{\vec{\delta}} (J_{\mathbf{r}}\mathbf{S}_{\mathbf{r}+\vec{\delta}} + J_{\mathbf{r}-\vec{\delta}}\mathbf{S}_{\mathbf{r}-\vec{\delta}}) \\ &\quad + \sum_{\vec{\delta}} (D_{\mathbf{r}}\mathbf{S}_{\mathbf{r}+\vec{\delta}} \times \vec{\delta} - D_{\mathbf{r}-\vec{\delta}}\mathbf{S}_{\mathbf{r}-\vec{\delta}} \times \vec{\delta}) + B\mathbf{e}_z.\end{aligned} \tag{12}$$

The current term in the LLG equation $-\sum_{\vec{\delta}} j_{\vec{\delta}}\mathbf{S}_{\mathbf{r}} \times [(\mathbf{S}_{\mathbf{r}+\vec{\delta}} - \mathbf{S}_{\mathbf{r}-\vec{\delta}})/2 \times \mathbf{S}_{\mathbf{r}}]$ is the discrete version of the continuous term $-(\mathbf{j}\cdot\nabla)\mathbf{n}$ [23, 28–31], which originates from the adiabatic 'spin transfer torque' that describes the coupling between the local magnetic moments and the conducting electrons. Here we make the cross product with $\mathbf{S}_{\mathbf{r}}$ twice the finite difference term $(\mathbf{S}_{\mathbf{r}+\vec{\delta}} - \mathbf{S}_{\mathbf{r}-\vec{\delta}})/2$ to remove the parallel component with respect to $\mathbf{S}_{\mathbf{r}}$, so that the local spin module is conserved during the time evolution.

We simulate the dynamical pinning and depinning processes as follows: we use an N by N square lattice with periodic boundary condition; the site-dependent exchange strength and DM interaction

$$\begin{aligned} J_{\mathbf{r}} &= J_0 \left\{1 + \lambda \exp\left[-\frac{(x+1/2)^2 + (y+1/2)^2}{\xi^2}\right]\right\}, \\ \frac{D_{\mathbf{r}}}{J_{\mathbf{r}}} &= \sqrt{2}\tan(2\pi/d) \end{aligned} \tag{13}$$

are chosen to have a Gaussian profile, where J_0 is the discrete version of $J(\infty)$ in equation (3) and d is the wavelength of the chiral magnet on the lattice. Here we have shifted the position $\mathbf{r} = (x, y)$ in the definition of J to the center of the elemental plaquette in the square lattice $(x + 1/2, y + 1/2)$ so that the periodic boundary condition is satisfied. We numerically integrate the LLG equation using the fourth-order Runge–Kutta method and calculate the position of the skyrmion and the total energy of the lattice at selected times. The time-step $\mathrm{d}t = 0.001$ is chosen to be small enough for our study and the simulation is performed from $t = 0$ to $t = 1000$.

3.2. The pinning process

We first choose $N = 40$, $J_0 = 4$, $\lambda = 0.5$, $\xi = 8$, $d = 18$, $B = 0.9$, and $\alpha = 0.2$ with zero current. For the initial condition, we put a single skyrmion at position $x = 16$ and $y = 0$, which has an offset from the pinning center $x = y = 0$. The result of the time evolution is that the skyrmion undergoes a circular motion around the pinning center with the distance to the pinning center becoming smaller and smaller, and finally stays at the pinning center (figure 3).

We have the following heuristic explanation of this process. Because the pinned skyrmion has lower energy than a free skyrmion and the LLG equation has a damping term, the offset skyrmion has a tendency to move to the pinning center. If we treat a skyrmion as a point particle, the LLG dynamics of this single skyrmion has an effective kinetic term that gives transverse motion related to the pinning force [30]; that is, skyrmion motion is not parallel to the 'attractive force' of the pinning center but makes an angle to the direction of the force. Combining the above two factors we get a circular motion with smaller and smaller distance from the pinning center.

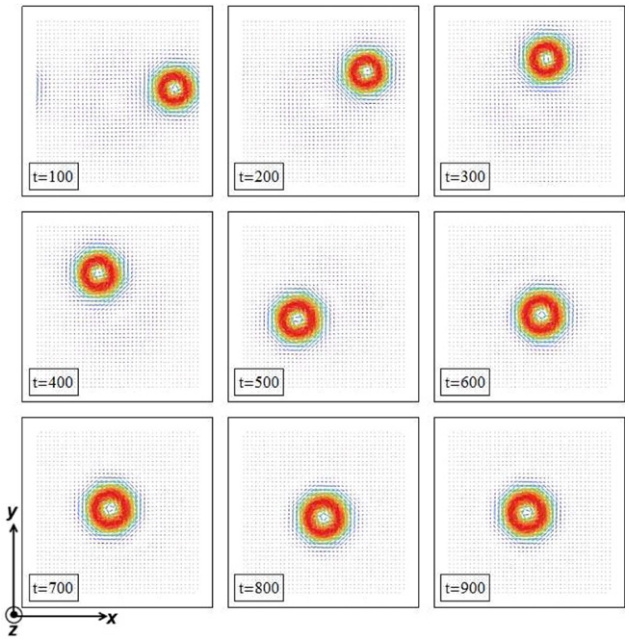

Figure 3. Snapshots of the Landau–Lifshitz–Gilbert dynamics of a skyrmion around a pinning center on a 40×40 lattice. The pinning center is at the origin point (0, 0). Initially we put a skyrmion at (16, 0), then the offset skyrmion undergoes a circular motion around the pinning center and finally stays at the pinning center.

In figure 4 we show the evolution of the system energy (minus the energy of the ferromagnetic state) versus time and the trajectory of the skyrmion in the pinning process. We can see that the system energy decreases with time; this is caused by the damping term in the LLG equation.

3.3. The depinning process

Now we study the depinning process so as to 'kick' a skyrmion out from the pinning center. Because a pinned skyrmion has lower energy than a free one, to depin a skyrmion we need to do positive work to it. In order to do work to a spin system, we can use a time-varying magnetic field or an applied adiabatic electric current. The magnetic field method is often used to sustain certain eigenmodes of the spin system near the ground state. According to Mochizuki [18], a time-varying in/out-of plane magnetic field with a certain frequency can trigger the rotating/breathing internal mode of a single skyrmion. In this paper, we choose the electric current method to push the pinned skyrmion.

To simulate the depinning process, we apply a square-current pulse of the form $\mathbf{j}(t) = \mathbf{j}_0\Theta(t)\Theta(t_{\rm f} - t)$ to the pinned

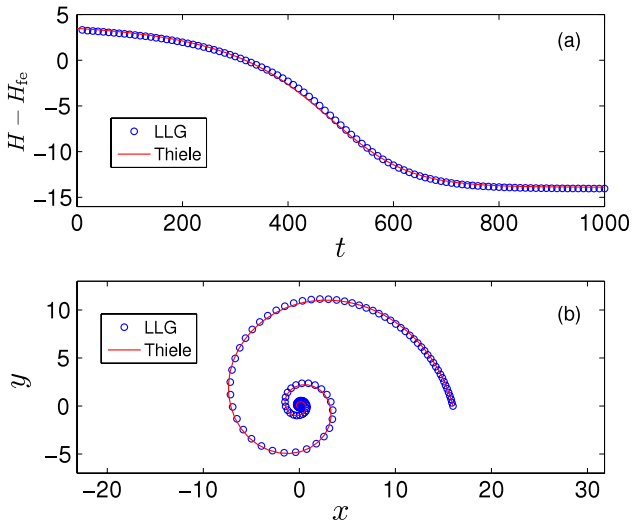

Figure 4. (a) System energy versus time for the pinning process. The energy decreases during the whole process and finally to a stationary value. (b) The pinning trajectory of the skyrmion. The skyrmion moves to the pinning center circularly. The results from LLG simulation (blue circle) and that from Thiele's equation (red curve) agree very well.

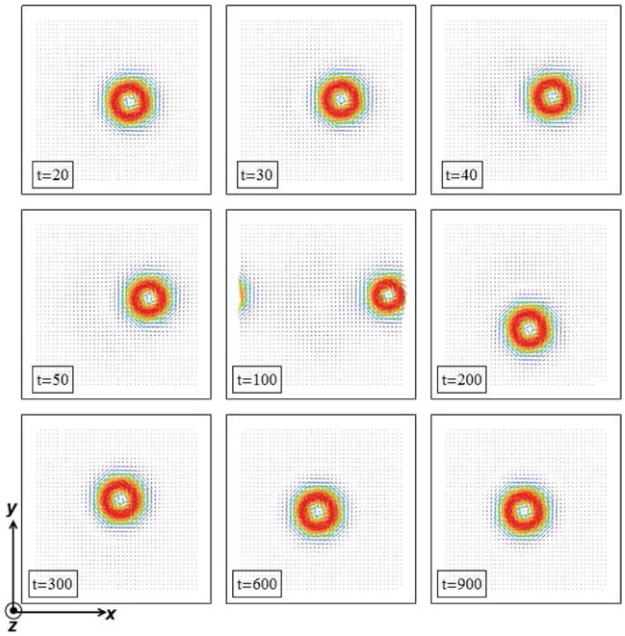

Figure 5. Snapshots of the Landau–Lifshitz–Gilbert dynamics with current for the depinning process. We apply current $\mathbf{j} = (0.2, -0.1)$ to the pinned skyrmion and the skyrmion moves and leaves the unit cell from the right boundary and enters the next unit cell from the left boundary. Then the current is turned off (at $t_f = 200$) and the skyrmion is attracted by the new pinning center and finally is pinned again. After the whole process the system state returns to the initial one. But in fact the skyrmion is pinned by another pinning center because we used a periodic boundary condition.

skyrmion configuration, where t_f is the time when we stop the current and $\Theta(t)$ is the Heaviside step-function.

We have adopted a periodic boundary condition in our simulation of the LLG equation, so we are implicitly simulating an infinite pinning center lattice in which each pinning center lies at the origin point of our simulated N by N unit cell. We expect the following phenomenon for the depinning process. When the current is turned on, the pinned skyrmion is pushed by the current to move. The direction of the skyrmion motion is determined by (1) the pinning force, (2) the pushing force (spin torque) of the current and (3) the tendency of the skyrmion to move transversely to the forces. Let the direction of skyrmion motion to be in the x-direction. At some time the skyrmion would leave the unit cell from the right boundary then enter the next unit cell from the left boundary and then move to the pinning center in this unit cell. Roughly at this time we turn off the current so the skyrmion is attracted by the pinning center in this unit cell. Just like the above pinning process, the skyrmion makes a circular motion and finally stays at the new pinning center.

To simulate this process, we use the parameters $\mathbf{j}_0 = (0.2, -0.1)$, $t_f = 200$ and other parameters that are the same as in the pinning simulation. We choose the current to be not parallel to the x-direction so that the skyrmion moves approximately in the x-direction. The numerical result is in agreement with our expectation (figure 5).

In figure 6(a) we show the evolution of system energy versus time. The system energy first increases and then decreases when the current is applied, but always decreases when the current is turned off. This is because the current could do positive or negative work to the skyrmion depending on whether the current is pushing the skyrmion away from or toward a pinning center. But it is the positive work done by the current that depins the skyrmion. Due to the damping, the system energy must decrease in the absence of the current. The trajectory of skyrmion motion in the whole process is shown in figure 6(b), where the black dashed line indicates the boundary of two successive unit cells of the simulated periodic lattice.

3.4. Thiele's equation for pinning and depinning

To gain more understanding of the previous results from LLG simulation, we follow the method of Thiele [33] to derive a force equation (Thiele's equation) from the torque equation (LLG). This equation incorporates both the attractive force from the pinning center and the electric current pushing force, which reads

$$G\mathbf{e}_z \times \mathbf{V} + \mathbf{F} - G\mathbf{e}_z \times \mathbf{j} - \alpha\eta\mathbf{V} = 0, \tag{14}$$

where $\mathbf{V} = \partial_t \mathbf{R}$ is the velocity of the skyrmion with $\mathbf{R}$ the position of the center of the skyrmion, $G = \int \mathrm{d}x\mathrm{d}y\, \mathbf{S} \cdot (\partial_x \mathbf{S} \times \partial_y \mathbf{S}) = -4\pi$ the effective charge of the (anti-)skyrmion in our simulation, $\mathbf{F} = -\nabla U$ the attractive force from the pinning potential U, $\mathbf{j}$ the electric current, α the Gilbert damping and $\eta = \int \mathrm{d}x\mathrm{d}y(\partial_x \mathbf{S})^2 = \int \mathrm{d}x\mathrm{d}y(\partial_y \mathbf{S})^2$ the shape factor of the skyrmion.

The various terms in equation (14) have the following physical meanings. The first term is the gyro-term, which can also be derived from the spin Berry phase integrated in a skyrmion [34]. If the electric current $\mathbf{j}$ and damping α are

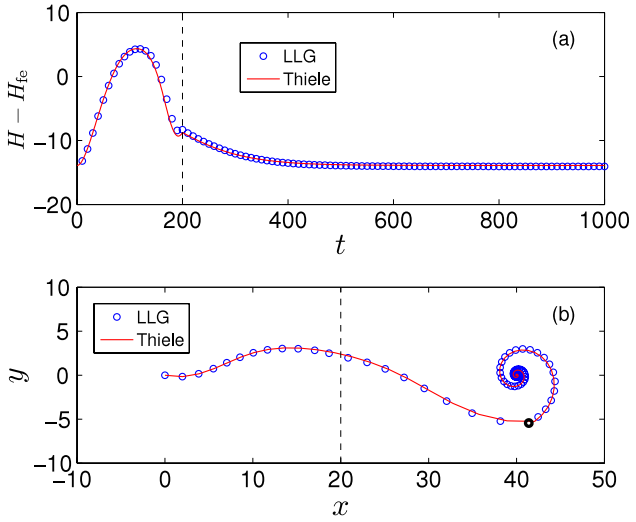

Figure 6. The evolution of the system energy versus time (a) and the depinning–pinning trajectory of the skyrmion (b). The current is turned on at $t = 0$ and the work done by the current enhances the system energy. After the current is turned off at $t = 200$, the system energy starts to decrease because of the damping, and finally reaches a stationary value, which is the initial value. After the whole process the system state returns to the initial state. In this process the skyrmion travels through the boundary of the simulated unit cell (black dashed line). The trajectory from LLG simulation (blue circle) and that obtained by Thiele's equation (red curve) agree very well. The bold black circle in (b) shows the position of the skyrmion at $t_f = 200$.

both zero, this term makes the skyrmion move perpendicularly to the applied forces. The second term is the applied force, which in our case is the attractive force exerted by the pinning potential. The third term is the electric current term, which pushes the skyrmion to move parallel to the applied current in the case of zero applied force and zero damping. The fourth term is the damping term, which makes the skyrmion move to lower energy regions.

Now we try to fit the results from LLG by Thiele's equation (14). For the pinning process, the phenomenological parameters we choose are $U(x, y) = -18.9\exp[-(x^2 + y^2)/100] + 5$, which is again a Gaussian function, but the range of decay (which is 10) is fitted to be different from that of magnetic exchange J (which is 8). This is because the size of the pinning potential is comparable to the size of the skyrmion, so we are not in the point particle limit in which the skyrmion size is much smaller than the typical length scale of the variation of potential. In the pinning process, the electric current is set to zero. The Gilbert damping is 0.2 as in the LLG simulation and the shape factor η is fitted to be $\eta = 16.0$, which is very close to the lattice sum $\sum_{\mathbf{r}}(\mathbf{S}_{\mathbf{r}+\mathbf{e}_x} - \mathbf{S}_{\mathbf{r}})^2 = 15.0$ from LLG simulation. With this set of parameters, the energy evolution and the trajectory of the skyrmion for the pinning process is very well fitted, as shown by the red curves in figure 4. For the depinning process, we use $U(x, y) + U(x - 40, y)$ to represent two neighboring pinning centers. The shape factor η is the same as for the pinning process. The current is set to $\mathbf{j} = 0.97\Theta(t)\Theta(200 - t)(0.2, -0.1, 0)$, which is 97% of that in LLG simulation. Again, the results show excellent agreement with that of LLG (see figure 6).

Besides the adiabatic STT term in our LLG equation (11), in conducting chiral magnets, there is another current-related term which is the so-called 'non-adiabatic spin-torque term' [28, 29, 31]. Combining the two terms we should make a change to the LLG as

$$(\mathbf{j}\cdot\nabla)\mathbf{S} \to (\mathbf{j}\cdot\nabla)\mathbf{S} + \beta\mathbf{S}\times[(\mathbf{j}\cdot\nabla)\mathbf{S}], \tag{15}$$

where β represents the strength of the non-adiabatic torque. It is known that this term alters the trajectory of single skyrmions. When there is no pinning center, the skyrmion would move parallel to the applied current if the value β is equal to the Gilbert damping α, otherwise the skyrmion motion would have a transverse component to the right/left of the current direction if β is larger/smaller than α [31]. This property could also be understood by Thiele's equation, after changing the current term in LLG, the corresponding current-related term in Thiele's equation is changed by

$$\begin{aligned} -G\mathbf{e}_z\times\mathbf{j} &\to -G\mathbf{e}_z\times\mathbf{j} + \beta\eta\mathbf{j} \\ &= -G\mathbf{e}_z\times\left(\mathbf{j} + \frac{\beta\eta}{G}\mathbf{e}_z\times\mathbf{j}\right). \end{aligned} \tag{16}$$

From the above equation, when $\alpha = \beta$ and $\mathbf{V} = \mathbf{j}$, the non-adiabatic term cancels the damping term. Furthermore, we can see that adding the non-adiabatic term is equivalent to re-defining the current in the adiabatic term. Therefore, in the following discussions, we can safely ignore the non-adiabatic term.

As a conclusion, even though we are not in the point particle limit, Thiele's equation still captures all the essential physics of the dynamics of skyrmion motion. This is partly due to the rigidity of the skyrmion, because it is both topologically stable and energetically favorable.

3.5. Critical current of the depinning process

In our simulations we found that, if the applied current is not large enough, the pinned skyrmion would not travel to other pinning centers but instead circulates around its own pinning position and finally stays at a nearby position. This means there is a threshold critical current to depin a skyrmion.

To study the critical current of depinning, we carry out a series of simulations with increasing current intensity $\mathbf{j} = \mu(0.2, -0.1)$ with $\mu = 0.51, \ldots, 0.55$ for a pinning strength $\lambda = 0.5$. The result shows that there exists a critical current below which the skyrmion cannot escape from the pinning center but circulates around the pinning center, and the energy will not exceed the barrier energy set by the pinning center; however, when the current is larger than the critical current, the skyrmion could escape from the pinning center and the energy exceeds the barrier energy (figure 7).

We further simulate the depinning processes for different pinning strengths λ and we find an almost linear dependence of the critical current $\mathbf{j}_c = \mu(0.2, -0.1)$ with respect to the pinning strength (figure 7(c)). The approximate relation is $\mu \approx \lambda$ in our dimensionless unit system.

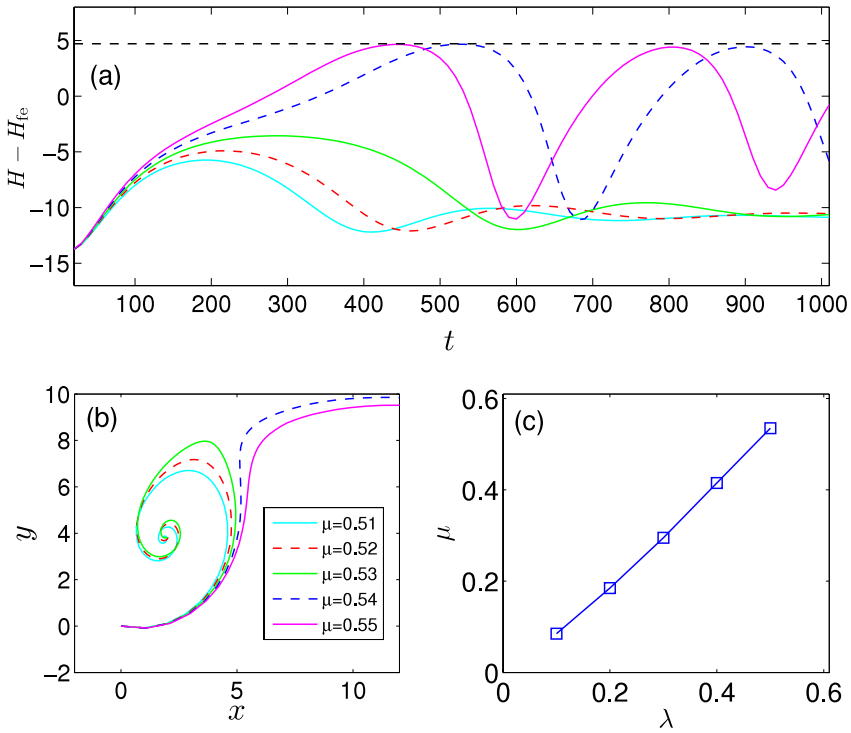

Figure 7. Energy evolution (a) and skyrmion trajectory (b) in different applied currents. For low currents up to $\mu = 0.53$ the skyrmion cannot escape from the pinning center at the origin point (0, 0) and the system energy cannot exceed the barrier indicated by the dashed line at roughly $H - H_{fe} = 4.7$. When the current is as large as $\mu = 0.54$, the skyrmion escapes from the pinning center and the depinning–pinning process happens several times because we do not turn off the current in this simulation, so the system energy has a large oscillation. (Parameters: $\lambda = 0.5$ and $\xi = 8$.) (c) Critical current versus pinning strength. The critical current $\mathbf{j}_c = \mu(0.2, -0.1)$ needed to depin a skyrmion varies almost linearly with respect to the pinning strength λ.

To estimate the critical current, we rescale the LLG in real material to our dimensionless form. We use letters with a prime to represent physical quantities in real material. First we carry out space rescaling, supposing the real material has magnetic exchange J' and crystal lattice spacing a'; then, because the magnetic exchange scales as the inverse square of length, we have $a^2 J = a'^2 J'$. Here J is the rescaled magnetic exchange for our simulated space unit defined by $18a \approx \lambda'$, where λ' is the helical wavelength in real material. Next we carry out time rescaling; in our simulation we have implicitly chosen the time unit to be $t_0 = 4\hbar/J$. After these rescalings, the unit of the electric current is $j_0 = (S/p)[q_e/(a^2 t_0)]$, where S is the spin quantum number of the local magnetic moment and p is the fraction of spin polarization of the electric current. Next we substitute real parameters chosen as $a' = 0.4$ nm, $J' \approx 3$ meV, $\lambda' \approx 60$ nm, $p \approx 0.1$ and $S \approx 1$ [31], then we get $j_0 \approx 2.4 \times 10^9$ A m^{-2}. With the above result we have $j_c \approx 5.3\lambda \times 10^8$ A m^{-2} (here λ refers to the pinning strength with order of magnitude 10^{-1} in our simulation) and the typical pinning and depinning time around $1000t_0 \approx 10$ ns.

The existence of critical current can also be understood by Thiele's equation. If the force from the current and that from the pinning potential balance each other, that is $\mathbf{F} - G\mathbf{e}_z \times \mathbf{j} = 0$, then the skyrmion ceases to move. Moreover, the equilibrium position of the skyrmion satisfies $\mathbf{R}_{eq} \parallel \mathbf{F} \perp \mathbf{j}$. So if the current is so large that the above force balance condition is never met, the skyrmion will escape from the pinning center.

4. Summary and outlook

We proposed a mechanism to pin skyrmions by introducing local maxima of magnetic exchange strength as pinning centers in the conventional Heisenberg spin model with DM interaction. Physically, the local maxima of exchange strength can be realized by local maxima of the density of itinerant electrons in the material. We studied the effect of this pinning center by stationary state analysis of the energy functional and found that it makes an isolated skyrmion more stable by lowering the skyrmion's core energy.

Besides the stationary state analysis, we also studied the dynamics of the chiral magnet with pinning centers by the LLG equation with a current term. We found that an offset skyrmion near a pinning center is attracted by it and undergoes a circular motion then finally stays at the pinning center. This pinned skyrmion can further be depinned by an applied current pulse, which pushes the skyrmion away from the pinning center so that the skyrmion can be attracted by other pinning centers. The above results are verified by a Thiele equation analysis. Our simulation showed that there exists a critical current below which the pinned skyrmion cannot escape from the pinning center. We carried out a series of simulations and found that the critical current, which is estimated to have order of magnitude 10^7–10^8 A m^{-2}, depends approximately linearly on the pinning strength. With the pinning and depinning processes, we actually found a way to manipulate the spacial positions of skyrmions in an

artificially made pinning center lattice. This pinning center lattice is expected to be realized by putting patterned metal grains on the surface of a chiral magnetic thin film.

Our pinning and depinning mechanism resembles in spirit the 'magnetic domain-wall racetrack memory' [32], in which patterned notches along the edges of the racetrack are used to pin the domain-walls and electric current pulses are used to depin them so that the information can 'flow'. A racetrack memory is constituted of a writing unit, a racetrack and a reading unit. For skyrmions, the writing unit could be realized by the method of 'skyrmion generation by a circular current' [31]. Our work could be considered as a model of the two-dimensional racetrack for skyrmions.

The critical current to depin skyrmions from material disorder is of order 10^6 A m^{-2} [20], which is much smaller than our estimated critical current to depin skyrmions from an artificially made pinning center 10^8 A m^{-2}. The above two values are both much smaller than the critical current in racetrack memory, which is of order 10^{12} A m^{-2}. Skyrmions in conducting chiral magnets can be more easily depinned and cause much smaller Joule heating for potential application.

Acknowledgments

This work is supported by NSFC (grant No 11074216). The authors thank J H Han for careful reading of the initial manuscript and fruitful suggestions.

References

[1] Skyrme T H R 1962 *Nucl. Phys.* B **31** 556
[2] Rajaraman R 1982 *Solitons and Instantons* (Amsterdam: North-Holland)
[3] Bogdanov A and Hubert A 1994 *J. Magn. Magn. Mater.* **138** 255
[4] Bogdanov A and Hubert A 1999 *J. Magn. Magn. Mater.* **195** 182
[5] Rößler U K, Bogdanov A N and Pfleiderer C 2006 *Nature* **442** 797
[6] Pappas C, Lelièvre-Berna E, Falus P, Bentley P M, Moskvin E, Grigoriev S, Fouquet P and Farago B 2009 *Phys. Rev. Lett.* **102** 197202
[7] Mühlbauer S, Binz B, Jonietz F, Pfleiderer C, Rosch A, Neubauer A, Georgii R and Böni P 2009 *Science* **323** 915
[8] Yu X Z, Onose Y, Kanazawa N, Park J H, Han J H, Matsui Y, Nagaosa N and Tokura Y 2010 *Nature* **465** 901
[9] Yu X Z, Kanazawa N, Onose Y, Kimoto K, Zhang W Z, Ishiwata S, Matsui Y and Tokura Y 2011 *Nature Mater.* **10** 106
[10] Heinze S, von Bergmann K, Menzel M, Brede J, Kubetzka A, Wiesendanger R, Bihlmayer G and Blügel S 2011 *Nature Phys.* **7** 713
[11] Seki S, Yu X Z, Ishiwata S and Tokura Y 2012 *Science* **336** 198
[12] Butenko A B, Leonov A A, Rößler U K and Bogdanov A N 2010 *Phys. Rev.* B **82** 052403
[13] Dzyaloshinsky I 1958 *J. Phys. Chem. Solids* **4** 241
[14] Moriya T 1960 *Phys. Rev.* **120** 91
[15] Shekhtman L, Entin-Wohlman O and Aharony A 1992 *Phys. Rev. Lett.* **69** 836
[16] Han J H, Zang J, Yang Z, Park J H and Nagaosa N 2010 *Phys. Rev.* B **82** 094429
[17] Li Y Q, Liu Y H and Zhou Y 2011 *Phys. Rev.* B **84** 205123
[18] Mochizuki M 2012 *Phys. Rev. Lett.* **108** 017601
[19] Petrova O and Tchernyshyov O 2011 *Phys. Rev.* B **84** 214433
[20] Schulz T, Ritz R, Bauer A, Halder M, Wagner M, Franz C, Pfleiderer C, Everschor K, Garst M and Rosch A 2012 *Nature Phys.* **8** 301
[21] Lee M, Kang W, Onose Y, Tokura Y and Ong N P 2009 *Phys. Rev. Lett.* **102** 186601
[22] Neubauer A, Pfleiderer C, Binz B, Rosch A, Ritz R, Niklowitz P G and Böni P 2009 *Phys. Rev. Lett.* **102** 186602
[23] Zhang S and Li Z 2004 *Phys. Rev. Lett.* **93** 127204
[24] Tatara G and Kohno H 2004 *Phys. Rev. Lett.* **92** 086601
[25] Barnes S E and Maekawa S 2005 *Phys. Rev. Lett.* **95** 107204
[26] Zhang S and Zhang S S L 2009 *Phys. Rev. Lett.* **102** 086601
[27] Jonietz F *et al* 2010 *Science* **330** 1648
[28] Everschor K, Garst M, Duine R A and Rosch A 2011 *Phys. Rev.* B **84** 064401
[29] Everschor K, Garst M, Binz B, Jonietz F, Mühlbauer S, Pfleiderer C and Rosch A 2012 *Phys. Rev.* B **86** 054432
[30] Zang J, Mostovoy M, Han J H and Nagaosa N 2011 *Phys. Rev. Lett.* **107** 136804
[31] Tchoe Y and Han J H 2012 *Phys. Rev.* B **85** 174416
[32] Parkin S S P, Hayashi M and Thomas L 2008 *Science* **320** 190
[33] Thiele A A 1972 *Phys. Rev. Lett.* **30** 230
[34] Stone M 1996 *Phys. Rev.* B **53** 16573